Jestr

Journal of Engineering Science and Technology Review 17 (1) (2024) 1 - 7

Research Article

JOURNAL OF
Engineering Science and Technology Review

www.jestr.org

Data-Driven Prediction and Optimization of Steam Biomass Gasification for Hydrogen Production using Nonlinear Autoregressive and Exogenous Inputs (NARx) Model

Mahlon Kida Marvin[1,*], Zakiyyu Muhammad Sarkinbaka[2] and Abdulhalim Musa Abubakar[3]

[1]*Department of Chemical Engineering, Faculty of Engineering, University of Maiduguri, Maiduguri, Nigeria*
[2]*Department of Chemical Engineering, Faculty of Engineering, Federal University Wukari, Wukari, Nigeria*
[3]*Department of Chemical Engineering, Faculty of Engineering, Modibbo Adama University, Yola, Nigeria*

Received 19 November 2023; Accepted 27 December 2023

Abstract

The application of machine learning (ML) in the prediction of hydrogen (H_2) production has proven to be an efficient tool for enhancing production capacity. However, while the reported algorithms have demonstrated robustness in hydrogen prediction, they fall short in capturing the dynamic nature of real-time production uncertainty. In this study, we proposed a dynamic data-driven algorithm for the identification and prediction of H_2 gas during an experimental steam gasification process. Initially, feature selection was conducted to assess the appropriateness of the data obtained from literature. Subsequently, a machine learning model, specifically based on the time series recurrent artificial neural network architecture, was developed to forecast the H_2 yield using predefined model inputs. To establish a benchmark for comparison, the machine learning model was optimized using the genetic algorithm (GA) optimizer to evaluate its predictive performance. The findings of the investigation revealed that the optimized NARx model exhibits robustness in predicting H_2 yields, achieving an R_2 value exceeding 0.90 and a Mean Squared Error (MSE) below 0.070, when evaluated against a predefined time trajectory. This stands in contrast to the performance of the reference NARx model, which yielded an R_2 below 0.90 and an MSE exceeding 0.40. This model could effectively be used to develop decision making strategy for large scale H_2 production from biomass gasification process.

Keywords: H_2 yield, Syngas, NARx, Genetic Algorithm, Biomass gasification

1. Introduction

Clean energy sources have experienced a notable surge in usage, witnessing a substantial 6% increase, with an additional 10% uptick observed between 2020 and 2021 [1], [2]. This upward trend is anticipated to persist, driven by a reduced reliance on fossil fuels, with an expected decline of 50% [3]. This shift reflects a growing global awareness and commitment to sustainable energy practices, fostering a more environmentally conscious approach to meet energy needs. As the world continues to prioritize cleaner alternatives, this trajectory underscores the ongoing transition towards a more sustainable and eco-friendly energy landscape [1], [2]. With this recent surge, there is a continuous effort to meet the growing energy demand by employing various mechanistic approaches through data-driven techniques.

H_2 fuel is increasingly being regarded as a sustainable alternative to traditional fossil fuels, primarily owing to its environmentally friendly characteristics and substantial energy capacity [3], Despite being the most abundant substance on earth, H_2 does not exist independently due to its highly reactive nature. Presently, approximately 50% of H_2 is produced from fossil fuel through a process known as steam reforming [4], [5]. Despite being the most cost-effective technique for H_2 production, this process is not environmentally friendly as it involves the emission of CO_2. Fossil fuels are nonrenewable and highly endothermic. Consequently, efforts have been made to explore alternative methods for H_2 production that are both efficient and sustainable. One such method is biomass gasification [6]. Biomass, which encompasses organic matter derived from various sources such as animal waste, wood waste, municipal waste, and oceanic plants, has the potential to generate clean H_2 with minimal emissions of SOx and NOx [5], [7], [8]. Several study on biomass gasification has been investigated for different biomass feedstock; biopolymers [9]–[12], algae [13]–[15], Municipal waste [16], [17], and food waste [18], [19].

Biomass gasification is primarily conducted through either thermochemical conversion or biochemical conversion. Thermochemical conversion encompasses combustion, gasification, pyrolysis, and liquefaction. On the other hand, biochemical conversion primarily involves extraction and hydrolysis [20]. Nevertheless, the thermochemical conversion of biomass is regarded as promising, given its efficiency and capacity for H_2 yield. This process of conversion uses heat as the primary mechanism for conversion [21]. Initially, biomass is subjected to steam for drying at a temperature of approximately 100°C before undergoing pyrolysis. In the pyrolysis stage, the feedstock is devolatilized at around 300°C, resulting in the production of char. Typically, the volatile products undergo a combustion process with oxygen, generating CO_2. The produced char then undergoes a gasification process by reacting with steam and CO_2 to yield H_2. The overall reaction pattern follows:

*E-mail address: mahlonkida@yahoo.com
ISSN: 1791-2377
doi:10.25103/jestr.171.01

Combustion: $C + O_2 \leftrightarrow CO_2$ $C + O_2 \leftrightarrow 2CO$

Pyrolysis: $CO + H_2O \leftrightarrow H_2 + CO_2$ $C + H_2O \leftrightarrow H_2 + CO$

Gasification: $C + \frac{1}{2}O_2 \leftrightarrow CO$ $C + 2H_2 \leftrightarrow CH_4$

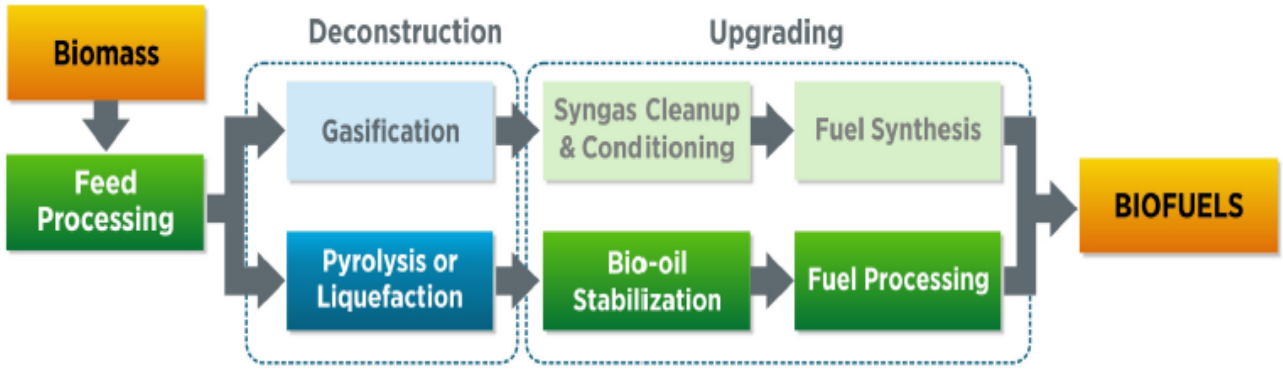

Fig. 1. Block flow for Thermochemical conversion of biomass

The investigation into H_2 production from biomass gasification through ML techniques has been explored [22]. Among ML methods, Artificial Neural Network (ANN) stands out as a common technique applied to address biomass gasification production [23]. In a related study [24], ANN was employed to predict the lower heating value of syngas from a modeled circulating fluidized bed (CFB) gasifier. Gibbs free energy was utilized in this study, assuming that all reactions occurred rapidly at chemical equilibrium. Elmaslar et al, [25] implemented four machine learning algorithms which includes linear regression, K-nearest neighbors, support vector machine, and decision trees to predict H_2 yield, utilizing seven predictors. The work of Mutlu et al, [26] involved classifier algorithms, such as the multi-class random forest and binary least square support vector machine classifier, to determine syngas composition. The random forest algorithm was also applied in predicting biochar yield from lignocellulosic biomass [27]. Other ML technique was recorded for biomass gasification process such as supercritical water gasification [28], and syngas exergy value investigation [29]. Recently, a paper reported the use of four ML models to predict the three-phase distribution of products from gasification [30]. However, while these algorithms have demonstrated robustness in syngas prediction, they fall short in capturing the dynamic nature of real-time production uncertainty. Furthermore, there is a notable gap in the literature regarding the application of time series ML models specifically for steam biomass gasification processes.

2. Methods

2.1 Data Collection and Preprocessing

Experimental data was retrieved from Singh et al, [31] for this study where a laboratory setup of gasification process was carried out in a fixed bed reactor. H_2 yield underwent continuous monitoring, with the steam flowrate (SFR) varied between 0.125 mL/min and 0.75 mL/min, and steam temperature ranging from 700°C to 800°C. To eliminate solid residues, the produced syngas was directed through a ceramic filter, and H_2 yield was determined by tracking the volumetric flowrate of the syngas post-filtration. Sampling occurred at 5-minute intervals, collecting both syngas and H_2. This study employed five gasification parameters to predict H_2 gas yield: steam flow rates (SFR), steam temperature (ST), syngas flowrate (GFR), Lower Heating Value (LHV), and Higher Heating Value (HHV). These variables were chosen based on their significant impact on H_2 yield during laboratory-scale production.

The methodology for this research is detailed in Figure 2. The collected data underwent feature selection and visualization to extract pertinent information influencing the model's performance. Table 1 outlines the initial data points used for model development. Data normalization was applied using min-max normalization to mitigate potential outliers and inconsistencies using;

$$X_{new} = \frac{x - \min(x)}{\max(x) - \min(x)} \quad (1)$$

Where X_{new} is the normalized data, x is the raw data. One advantage of this normalization technique is its ability to maintain the initial relationships among the original datasets while reducing its bounded range.

Table 1. First ten sample set of data used in this work

Time (min)	ST (°C)	GFR (mL/min)	SFR (mL/min)	LHV (MJ/Nm^3)	HHV (MJ/Nm^3)	SYNGAS m^3/kg	H_2 yield (%)
5	700	0.125	1.25	12.05295	13.03671	14.4599	20.81625
10	700	0.125	0.17	12.11715	13.41316	20.21863	25.5586
15	700	0.125	0.22	11.23842	12.42411	7.999975	44.28442
20	700	0.125	0.23	11.41197	12.5954	2.662519	54.78182
25	700	0.125	0.22	10.46062	11.54517	0.710389	53.65157
30	700	0.125	0.28	10.45667	11.5751	0	56.82829
35	700	0.125	0.23	10.41426	11.55376	0	57.92771
40	700	0.125	0.22	10.40344	11.55141	0	58.36982
45	700	0.125	0.18	10.38348	11.55717	0	59.70891
50	700	0.125	1.25	12.05295	13.03671	14.4599	20.81625

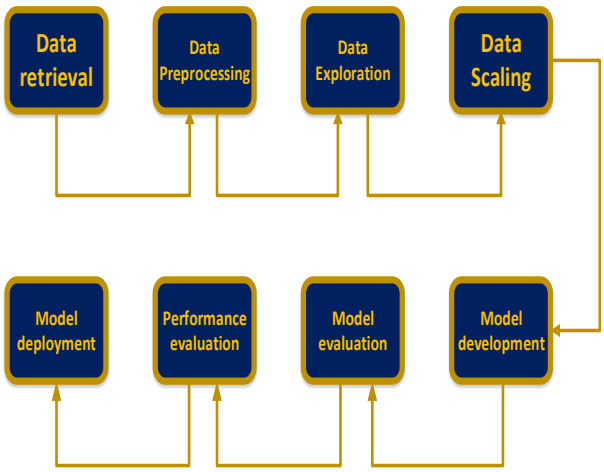

Fig. 2. Flow diagram for methodology

2.2 NARx Model Architecture

NARx was used as the prediction model, while GA optimizer was used to minimize the error derivative of the network by adjusting the weights. NARx is a recurrent neural network with feedback connection to the input layer with respect to time delay function n_u and n_y. Unlike other reported static ANN models, the strength of the NARx model lies in its ability to capture the uncertainty of time dependent data which makes it robust for dynamic modelling. The model follows an equation of the form:

$$y_{(t)} = f\left(y_{t-1}, y_{t-2}, \ldots . y_{t-n_y}, x_{t-1}, x_{t-2}, \ldots . . x_{t-n_u}\right) + \varepsilon_t \quad (2)$$

Where x_t is the input at time t, y_t is the response, ε_t is the training error at each time interval, f is a nonlinear function, n_u and n_y are the time lagged input and time lagged output respectively. Figure 3 shows the NARx architecture. It consists of an input layer, hidden layer with determinant weights w obtained through training and bias hyper parameter b, a feedback loop of the response variable y_t and an activation function g. The recurrent nature of the network follows a differential equation such as:

$$\tau \frac{dy_i}{dt} = -y_i + g\left(x_i + \sum_j w_i v_i\right) \quad (3)$$

τ is the time coefficient, $g( )$ is the activation function and is the output of the hidden neurons. Table 2 presents the parameters used for the model.

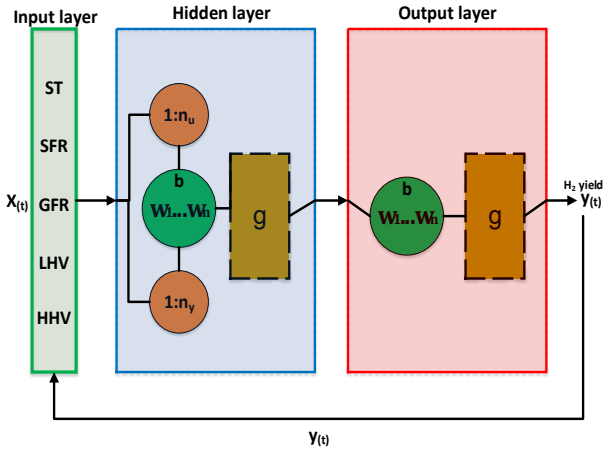

Fig. 3. NARx architecture

Table 2. Parameter used in this work

Parameter	Value
Number of hidden layer	1
Number of hidden neurons	10
Number of Input neurons	5
Activation function	Tansig
Time lag input	2
Time lag output	2
Learning rate	0.001

GA is coupled with the model to optimize the weights thereby minimizing the error derivative represented by the equation:

$$\frac{dE}{dy} = -(t^{(n)} - y^{(n)}) \quad (4)$$

Where $t^{(n)}$ represents the training target for n datasets and $y^{(n)}$ represents the approximated target for n datasets. The smaller the training error, the better the prediction ability of the model.

GA optimizer is a concept based on natural selection inspired by the Darwinian theory of evolution [32]. As shown in Figure 4, solutions are presented as population. For this case, the population are basically the weights of the NARx model which are initially chosen at random. These weights undergo a tournament selection where the optimum solutions are placed in a mating pool for crossover operation to generate new set of weight values which are called offspring. These offspring are further subjected for mutation to obtain new solutions and then selection of best fit is carried out to determine the best offspring. This process is done in an iterative manner until the best solutions (optimum weights) are obtained. The efficiency of GA lies in its ability to optimize a function around a global optimum and it does not require a derivative information. The pseudocode for the GA is given as follows:

NARx-GA *(P, y, m)*

Extract weights from developed NARx model; Initialize generation 0: k = 0;
P_k = P randomly generated weights; Evaluate P_k:
Compute fitness(i) for each I = = P_k;
Do
{
Create generation k+1:
*Select(1-y) * P members of P_k; Insert to P_k+1;*
Select y by n members of P_k; Produce offspring and insert to P_k+1;
Select m by n members of P_k+1; Invert a randomly selected bit for each member
Evaluate P_k+1 and compute fitness for each I;
}
While *fitness value is not high enough;* ***return*** *P_k*

P denotes the population size, y signifies the proportion of NARx weights replaced through crossover in each iteration, and m denotes the mutation rate.

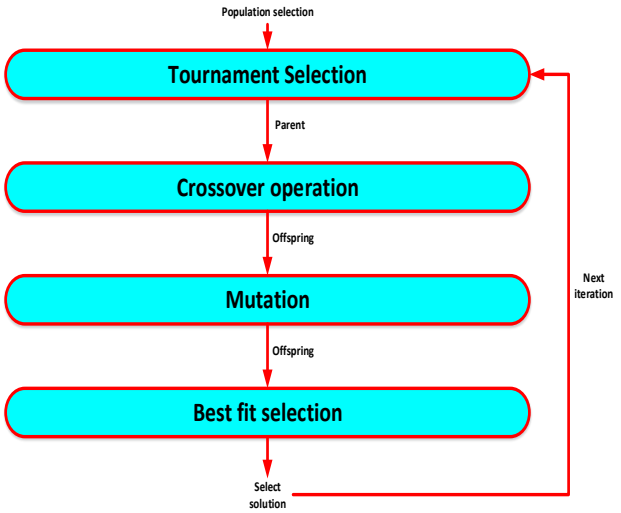

Fig. 4 Flow diagram for GA algorithm

2.3 Performance Evaluation

A comparative framework was established for the reference NARx model and the optimized (NARx-GA) model. The evaluation was conducted based on a set of performance indices outlined in this study, comprising the mean squared error (MSE), root mean squared error (RMSE), and multiple coefficients of determination (R^2). Throughout the training process, an iterative approach was employed to minimize the network error by adjusting the weights, as previously mentioned, and manipulating the number of hidden layer neurons.

The mean squared error (MSE) served as a metric during training, quantifying the error incurred. It represents the average square difference between the predicted response value and its actual counterpart, offering insights into the accuracy of the model's predictions. It is given by:

$$\text{MSE} = \frac{1}{\text{N}}\sum_{\text{n=1}}^{\text{N}}(\text{actual} - \text{predicted})^2 \quad (5)$$

where *N* is the overall amount of data. The root mean squared error (RMSE) is calculated between the measured values and the predicted values using:

$$\text{RMSE} = \sqrt{\frac{1}{\text{N}}\sum_{\text{n=1}}^{\text{N}}(\text{actual} - \text{predicted})^2} \quad (6)$$

Coefficient of determination, R^2 expresses the proportion of the total variation in response variable (predicted value) that is explained by different independent variables. It is given by the equation:

$$R^2 = 1 - \frac{\sum_{n=1}^{n}(actual-predicted)^2}{\sum_{n=1}^{n}(average-predicted)^2} \quad (7)$$

The lower the difference between actual and forecast values the higher the value of the determination coefficient. The value of R^2 is between 1 and 0. R^2 is near 1, for a good fit model, and R^2 near 0 indicates a poor fit model.

3. Results and Discussion

3.1 Data Reliability Analysis

This section presents the outcomes derived from the feature selection process. To construct the NARx model, a series of pairwise feature correlation charts were generated, specifically depicted in Figures 5 and 6 for H_2 yield. These charts visually outline the degree of discrepancy between each variable in the dataset and illustrate their interrelationships. Through careful examination of these charts, the feature relationships between predictors and the response variable are studied, providing valuable insights into the correlations shaping the dataset.

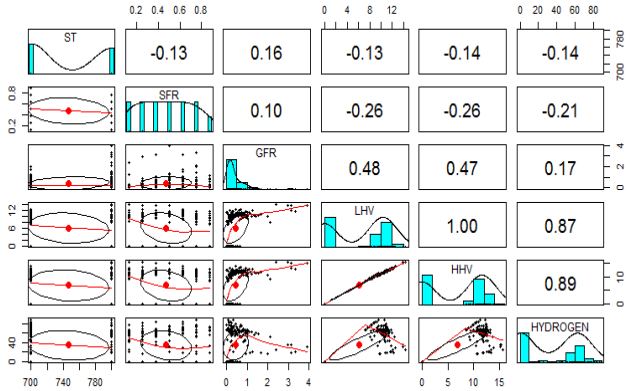

Fig. 5 Pairwise correlation between predictors and H_2

From figure 5, the upper diagonal presents the correlation matrix. Usually, the correlation matrix lies between -1 which indicates a perfectly less correlation between each feature, and +1 which indicates a perfectly good correlation. It is evident that the variables are correlated judging from the plot. It can be seen that GFR, LHV and HHV are positively and near perfectly related to H_2 yield, whereas, ST and SFR are negatively related to H_2 yield with a value of -0.14 and -0.21. Usually, a negative correlation occurs due to large numeric disparities between features values hence, data normalization was carried out to avoid inaccuracies in the predictive ability of the NARx model. From the lower diagonal of the correlation plots, it can be seen that the values of each variable follow a similar pattern which indicates the response of each variable to its corresponding feature. The histograms in the diagonal indicates the level of outliers for each parameter. It is observed from the histogram that there are fewer possibilities of outliers recorded. The lower diagonal indicates the pattern that exist between a variable and the output parameter. From table 3, the possibly of outliers are seen from the mean and median of each feature. H_2 yield, GFR, LHV and HHV has an obvious outlier compared to ST and SFR. As seen in Figure 7, there is a consistent flowrate for H_2 yield despite recording a lower steam flowrate. While at a steam to biomass ration of 1.50, the upper diagonal presented a strong interaction between the lower and higher heating value to the effectual yield of H_2. This is part of the evidence obtained from the experimental study obtained in [31], where a syngas flowrate between 0.325mL/min and 0.75mL/min was obtained at a temperature 700°C and SFR of 0.125mL/min and 0.25mL/min respectively. Similarly, the lower diagonal in Figure 6 also indicates the pattern of relationship between the input and output variable. Figure 7 presents a response plot for H_2 yield. Major clusters are formed close to higher H_2 yield for both LHV and HHV while a dispersed pattern at specific intervals is recorded for SFR indicating a timely change in the collection yield of H_2.

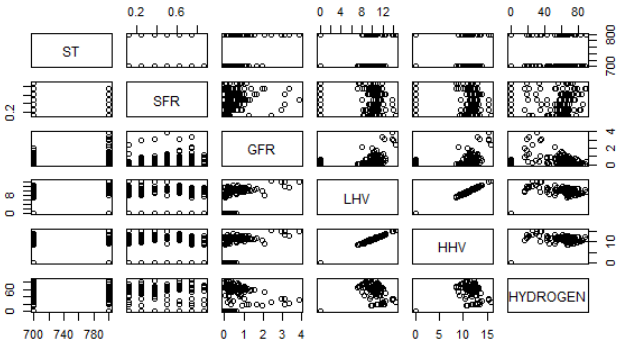

Fig. 6. Singular relationship for predictors and H_2

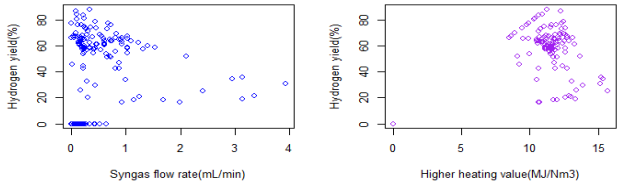

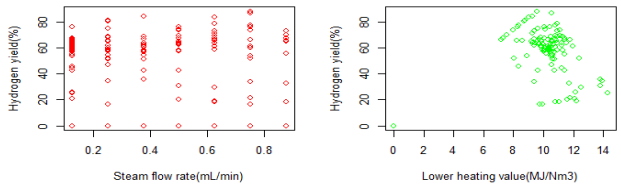

Fig. 7. Response plot for H_2 yield

The distribution of lower and higher heating values throughout the production period appears uniform. Notably, an increase in the moderately higher heating value correlates with an augmented yield of H_2. Syngas flowrate exhibits a relatively modest impact on H_2 yield, with the yield reaching its maximum irrespective of the flowrate. On the other hand, steam flowrate emerges as a more influential factor affecting H_2 yield. The analysis demonstrates that H_2 yield is notably sensitive to steam flowrate (SFR), lower heating value (LHV), higher heating value (HHV), syngas flowrate (GFR), and steam temperature (ST). Consequently, all five predictors will be incorporated in the neural network for H_2 yield prediction.

Table 3. Outlier Investigation for feature parameters

	ST (°C)	GFR (mL/min)	SFR (mL/min)	LHV (MJ/Nm^3)	HHV (MJ/Nm^3)	SYNGAS m^3/kg	H_2 yield (%)
Minimum	700	0.00	0.13	0.00	0.00	0.00	0.00
Median	700	0.23	0.50	9.29	10.62	0.00	42.63
Mean	746	0.44	0.47	6.083	6.82	1.71	34.36
Maximum	800	3.92	0.88	14.28	15.69	23.05	88.36

3.2 NARx model evaluation

Figure 8 presents the actual and predicted trend which shows the timely change of H_2 yield with respect to the predictors. The residual discrepancy between the observed values and the predicted values is extremely small, approaching a high level of precision.

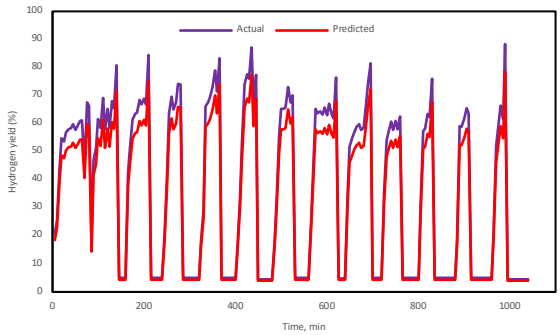

Fig. 8. Dynamic change of H_2 yield with respect to input variables

In Figure 9, the plot for the reference NARx model reveals an R^2 value of 0.890. The training accuracy is depicted at 0.925, while the validation accuracy hovers around 0.904. It is evident that overfitting did not occur, but a test accuracy of approximately 0.716 was achieved. This outcome suggests that the relationship between H_2 yield and the five predictors was not adequately captured, resulting in a model with fair performance. The recovery of H_2 yield was predominantly associated with the steam temperature injected into the reactor, wherein the flow of steam was notably influenced by the steam-to-biomass ratio. This practical correlation underscores the significance of modeling the relationship between predictors and responses accurately. Failure to capture appropriate measurements could lead to discrepancies in the feature selection of the NARx model.

In Figure 10, the regression fit for NARx-GA is illustrated. Remarkably, a training accuracy of 0.930 and a validation accuracy of 0.960 were achieved, resulting in an overall model performance of 0.941. These outcomes underscore the effectiveness of the global optimizer embedded in the model, indicating an optimal solution. The optimized NARx model demonstrates a superior ability to predict H_2 yield based on the provided predictor variables compared to the reference model. The incorporation of the global optimizer has evidently enhanced the predictive accuracy of the model.

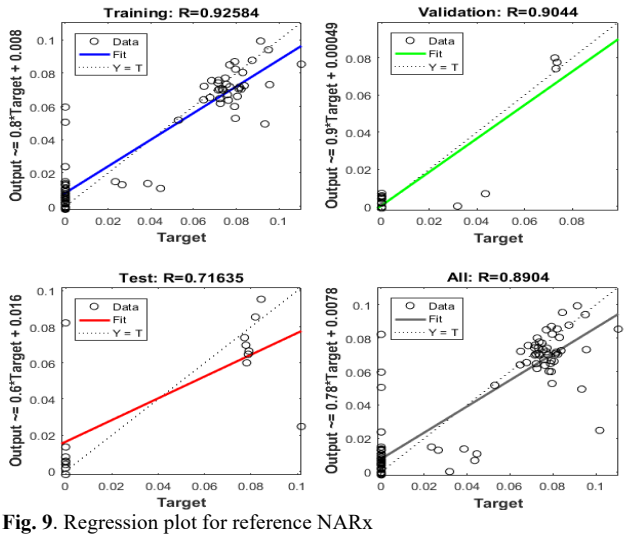

Fig. 9. Regression plot for reference NARx

As outlined in Table 3, a performance comparison between the NARx-GA and the reference NARx model is provided. The referenced NARx model exhibited an MSE of 0.477, whereas the NARx-GA model achieved a significantly reduced MSE of 0.056. This substantial difference underscores the robustness of the GA in enhancing the

predictive capability of the NARx model. Figure 11 illustrates the effective minimization of errors through the optimization of weights. As the error derivative approaches 0, the model accuracy improves, and NARx-GA proves to be particularly efficient in achieving this outcome.

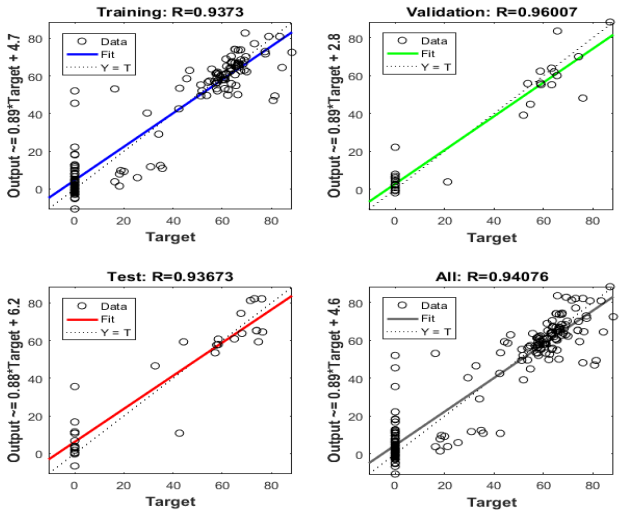

Fig. 10. Regression plot for NARx-Ga

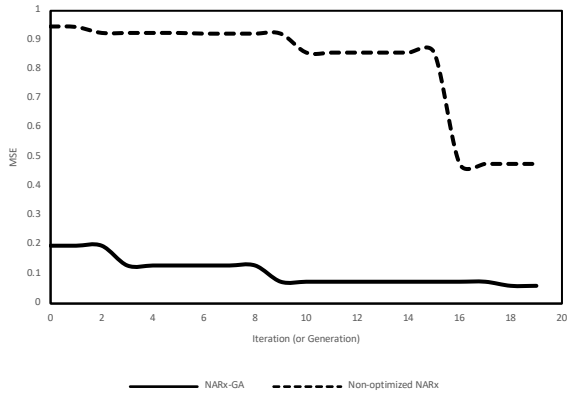

Fig. 11. MSE plot

Similarly, judging from the model accuracy between both compared models, NARx-GA outperformed reference NARx model with much difference. It can be observed however that the accuracy of the model could be improved by varying the number of hidden neurons or lag time of the NARx model. This is however noticed as H_2 yield is strongly dependent on the steam flow rate and temperature. The lower and higher heating value are shown to be of influence to the developed model through the non-monotonic trajectory of H_2 as shown in Figure 9. It is shown that GA increased the prediction accuracy of the NARx model by about 7.2% making it more robust and efficient. This indicates the efficiency of GA to improve the performance of the NARx model.

Table 3. Performance evaluation for models

	NARx-GA	Reference NARx
R^2	0.941	0.890
MSE	0.061	0.477
RMSE	0.237	0.691

4. Conclusions

The production of H_2 gas via biomass gasification has been shown to be a promising and efficient process. Several reports on how to improve the yield is one of the discussed topics in the field. In this work, a preliminary study was carried out on the data obtain from literature where a major determinant of the optimal operation is in its investigated data. Furthermore, a prediction model based on a hybrid ANN was developed on the heating value, steam flowrate, syngas flowrate and steam temperature of the biomass gasification process to determine the production of H_2 as the major target. Also, the developed model was optimized in terms of key performance indicators such as MSE and R^2 to investigate the model efficiency.

It was shown that NARx-GA has the robustness to predict the yield of H_2 (with $R^2 > 90\%$ and MSE < 0.070) on the basis of a set time trajectory as against the non-optimized NARx with $R^2 < 90\%$ and MSE > 0.40. It was shown by correlation that the yield of H_2 and other syngas was mostly influenced by the steam temperature, syngas and steam flowrates, and heating values. A correlation plot was used to indicate the strong relationship between feature values. GA is a global optimizer which makes efficient for global optimization problems. It has been proven effective in optimizing machine learning models which is why it is most common for optimizing machine learning models however, given the need to improve the predictive efficiencies of this model, it is recommended to implement some alternative global optimizers on the model and then compare their strengths.

Acknowledgment
The authors would like to appreciate the department of Chemical Engineering for it immerse contribution in the study of this paper. This study was supported in part by Clean Technology Hub, Abuja.

References

[1] A. K. Hossain and O. Badr, "Prospects of renewable energy utilisation for electricity generation in Bangladesh," *Renew. Sustain. Ener. Rev.*, vol. 11, no. 8, pp. 1617–1649, Oct. 2007, doi: 10.1016/j.rser.2005.12.010.

[2] L. Cao, K. M Iris, X. Xiong, D. C. Zhang, D. C. W. Tsang, S. Zhang, J. H. Clark, C. Hu, Y. Hau, J. Shang and Y. S. Ok., "Biorenewable hydrogen production through biomass gasification: A review and future prospects," *Environ. Res*, vol. 186, pp. 109547, Jul. 2020, doi: 10.1016/j.envres.2020.109547.

[3] H. O. Kargbo, J. Zhang, and A. N. Phan, "Optimisation of two-stage biomass gasification for hydrogen production via artificial neural network," *Appl. Energy*, vol. 302, pp. 117567, 15th Nov. 2021, doi: 10.1016/j.apenergy.2021.117567.

[4] L. Han, Q. Wang, Y. Yang, C. Yu, M. Fang, and Z. Luo, "Hydrogen production via CaO sorption enhanced anaerobic gasification of sawdust in a bubbling fluidized bed," *Int. J. Hydro. Energy*, vol. 36, no. 8, pp. 4820–4829, Apr. 2011, doi: 10.1016/j.ijhydene.2010.12.086.

[5] Y. H. Chan, K. W. Cheah, B. S. How, A. C. M. Loy, M. Shahbaz, H. K. G. Singh, N. R. Yusuf, A. F. A. Shuhaili, S. Yusup, W. A. W. A. Ghani, J. Rambli, Y. Kansha, H. L. Lam, B. H. Hong and S. L. Ngah, "An overview of biomass thermochemical conversion technologies

in Malaysia," *Sci. Tot. Env.*, vol. 680, pp. 105–123, Aug. 2019, doi: 10.1016/j.scitotenv.2019.04.211.

[6] M. R. Mahishi, M. S. Sadrameli, S. Vijayaraghavan, and D. Y. Goswami, "A Novel Approach to Enhance the Hydrogen Yield of Biomass Gasification Using CO_2 Sorbent," *J. Eng. Gas Turbine Power*, vol. 130, no. 1, pp. 1–8, Jan. 2008, doi: 10.1115/1.2747252.

[7] E. Shayan, V. Zare, and I. Mirzaee, "On the use of different gasification agents in a biomass fueled SOFC by integrated gasifier: A comparative exergo-economic evaluation and optimization," *Energy*, vol. 171, pp. 1126–1138, Mar. 2019, doi: 10.1016/j.energy.2019.01.095.

[8] Z. Khan, S. Yusup, and M. M. Ahmad, "Effect of Temperature and Steam to Biomass Ratio on NO and SO_2 Production in Palm Kernel Shell Catalytic Steam Gasification with In-situ situ CO_2 Adsorption," *2nd World Sustainability Forum*, pp. 1–10, Nov. 2012.

[9] A. Smolinski, N. Howaniec, and A. Bak, "Utilization of Energy Crops and Sewage Sludge in the Process of Co-Gasification for Sustainable hydrogen production," *Energies*, vol. 11, no. 4, Art. No. 809, Mar. 2018, doi: 10.3390/en11040809.

[10] A. Zubair, M. Rao, M. R. Somalu, A. Muchtar, S. A. Sulaiman and W. R. W. Daud, "Effect of particle size and temperature on gasification performance of coconut and palm kernel shells in downdraft fixed-bed reactor," *Energy*, vol. 175, pp. 931–940, May 2019, doi: 10.1016/j.energy.2019.03.138.

[11] Z. Khan, S. Yusup, P. Kamble, M. Naqvi, and I. Watson, "Assessment of energy flows and energy efficiencies in integrated catalytic adsorption steam gasification for hydrogen production," *Appl. Energy*, vol. 225, pp. 346–355, Sep. 2018, doi: 10.1016/j.apenergy.2018.05.020.

[12] H. L. Zhu, Y. S. Zhang, M. Materazzi, G. Aranda, D. J. L. Brett, P. R. Shearing and G. Manos, "Co-gasification of beech-wood and polyethylene in a fluidized-bed reactor," *Fuel Proc. Tech.*, vol. 190, pp. 29–37, Jul. 2019, doi: 10.1016/j.fuproc.2019.03.010.

[13] M. A. Adnan, Q. Xiong, A. Hidayat, and M. M. Hossain, "Gasification performance of Spirulina microalgae – A thermodynamic study with tar formation," *Fuel*, vol. 241, pp. 372–381, Apr. 2019, doi: 10.1016/j.fuel.2018.12.061.

[14] D. De Clercq, Z. Wen, and F. Fan, "Performance evaluation of restaurant food waste and biowaste to biogas pilot projects in China and implications for national policy," *J. Environ. Man.*, vol. 189, pp. 115–124, Mar. 2017, doi: 10.1016/j.jenvman.2016.12.030.

[15] A. Adnan and M. M. Hossain, "Gasification performance of various microalgae biomass – A thermodynamic study by considering tar formation using Aspen plus," *Ener. Conv. Man.*, vol. 165, pp. 783–793, Jun. 2018, doi: 10.1016/j.enconman.2018.03.078.

[16] Q. Shao, J. Li, S. Yang, and H. Sun, "Effects of different substrates on MEC anodic membrane Bio-diversity and hydrogen production performance," *Wat. Sci. & Tech.*, vol. 79, no. 6, pp. 1123–1133, May 2019, doi: 10.2166/wst.2019.107.

[17] D. Hoornweg, P. Bhada-Tata, and C. Kennedy, "Environment: Waste production must peak this century," *Nature*, vol. 502, no. 7473, pp. 615–617, Oct. 2013, doi: 10.1038/502615a.

[18] C. Yan, J. Wang, H. Du, L. Zhu, T. Jiang, H. Jiang, H. Wu and B. Wang, "Solar thermal electrochemical process (STEP) action to biomass: Solar thermo-coupled electrochemical synergy for efficient breaking of biomass to biofuels and hydrogen," *Ener. Conv. Man.*, vol. 180, pp. 1247–1259, Jan. 2019, doi: https://doi.org/10.1016/j.enconman.2018.11.056.

[19] X. Zheng, Z. Ying, B. Wang, and C. Chen, "CO_2-gasification of municipal solid waste (MSW) in a drop tube reactor: Experimental study, Thermodynamic analysis of syngas," *Energy & Fuels*, vol. 32, no. 4, pp. 5302 – 5312, Mar 2018, doi: 10.1021/acs.energyfuels.7b04133.

[20] T. Damartzis and A. Zabaniotou, "Thermochemical conversion of biomass to second generation biofuels through integrated process design — A review," *Renew. Sustain. Ener. Rev.*, vol. 15, no. 1, pp. 366–378, Jan. 2011, doi: 10.1016/j.rser.2010.08.003.

[21] USDE, "Thermochemical Conversion: Using Heat and Catalysis to Make biofuels and bioproducts," *US Department of Energy*, USA, pp. 1–4, 2017.

[22] A. G. Adeniyi, J. O. Ighalo, and G. Marques, "Utilisation of machine learning algorithms for the prediction of syngas composition from biomass bio-oil steam reforming," *Intern. J. Sustain. Ener.*, vol. 40, no. 4, pp. 1–16, Sep. 2021, doi: 10.1080/14786451.2020.1803862.

[23] S. Ascher, I. Watson, and S. You, "Machine Learning Methods for Modelling the Gasification and Pyrolysis of biomass and waste," *Renew. Sustain. Ener. Rev.*, vol. 155, Art. No. 111902, Mar. 2022, doi: 10.1016/j.rser.2021.111902.

[24] F. Kartal and U. Ozveren, "A deep learning approach for prediction of syngas lower heating value from CFB gasifier in Aspen plus ®," *Energy*, vol. 209, Art. No. 118457, Oct. 2020, doi: 10.1016/j.energy.2020.118457.

[25] E. Elmaslar, D. Aksu, A. Ongen, M. Ali, and H. K. Ozcan, "Hydrogen production via biomass gasification, and modeling by supervised machine learning algorithms," *Int. J. Hydro. Ener.*, vol. 44, no. 32, pp. 17260–17268, Jun. 2019, doi: 10.1016/j.ijhydene.2019.02.108.

[26] A. Y. Mutlu and O. Yucel, "An artificial intelligence-based approach to predicting syngas composition for downdraft biomass gasification," *Energy*, vol. 165, pp. 895 – 901, Dec. 2018, doi: 10.1016/j.energy.2018.09.131.

[27] X. Zhu, Y. Li, and X. Wang, "Machine learning prediction of biochar yield and carbon contents in biochar based on biomass characteristics and pyrolysis conditions," *Bio. Tech.*, vol. 288. May, Art. No. 121527, Sept. 2019, doi: 10.1016/j.biortech.2019.121527.

[28] J. Li, L. Pan, M. Suvarna, and X. Wang, "Machine learning aided supercritical water gasification for H2-rich syngas production with process optimization and catalyst screening," *Chem. Eng. J.*, vol. 426, pp. 131285, Dec. 2021, doi: https://doi.org/10.1016/j.cej.2021.131285.

[29] S. Sezer and U. Ozveren, "Investigation of syngas exergy value and hydrogen concentration in syngas from biomass gasification in a bubbling fluidized bed gasifier by using machine learning," *Int. J. Hydro. Ener.*, vol. 46, no. 39, pp. 20377 – 20396, Jun. 2021, doi: 10.1016/j.ijhydene.2021.03.184.

[30] J. Li, L. Li, Y. W. Tong, and X. Wang, "Understanding and optimizing the gasification of biomass waste with machine learning," *Green Chem. Eng.*, vol. 4, no. 1, pp. 123–133, Mar. 2023, doi: 10.1016/j.gce.2022.05.006.

[31] D. Singh, S. Yadav, N. Bharadwaj, and R. Verma, "Low temperature steam gasification to produce hydrogen rich gas from kitchen food waste: Influence of steam flow rate and temperature," *Int. J. Hydro. Ener.*, vol. 45, no. 41, pp. 20843 – 20850, Aug. 2020, doi: https://doi.org/10.1016/j.ijhydene.2020.05.168.

[32] Y. Chang, J. Lin, J. Shieh, and M. F. Abbod, "Optimization the Initial Weights of Artificial Neural Networks via Genetic Algorithm Applied to Hip Bone Fracture Prediction," *Adv. Fuzz. Syst.*, vol. 2012, no. 6, Art. No. 6, Jan. 2012, doi: 10.1155/2012/951247.